



Characterization of deformation localization in cold-rolled metastable β -Ti–Nb–Ta–Zr alloy

X.M. Ma, W. Sun*

Institute of Microstructure and Property of Advanced Materials, Beijing University of Technology, 100 Pingle Yuan, Chaoyang District, Beijing 100124, China

ARTICLE INFO

Article history:

Received 4 July 2010

Received in revised form

16 November 2010

Accepted 14 January 2011

Available online 22 January 2011

Keywords:

Ti–Nb–Ta–Zr alloy

Cold rolling

Deformation band

Transmission electron microscopy

ABSTRACT

The deformation-induced microstructural variation in the metastable β -type biomedical Ti–35Nb–5Ta–7Zr (wt.%) alloy subjected to multi-pass cold-rolling to 90% reduction has been investigated by a combination of X-ray diffraction, optical microscopy, conventional transmission electron microscopy (TEM) and high-resolution transmission electron microscopy (HRTEM) techniques. Multi-pass cold rolling for the Ti–35Nb–5Ta–7Zr alloy includes various localized deformation processes which can result in dislocation tangle, stress-induced ω -phase transformation and deformation-band formation. Deformation-induced amorphization caused by high-density defect accumulation in deformation bands has been identified. By means of TEM and HRTEM observations, distributional, morphological and structural features for deformation bands have been clearly revealed.

© 2011 Elsevier B.V. All rights reserved.

1. Introduction

Metastable β -type titanium alloys are promising candidates for serving as bio-implant materials of human hard tissues (such as bone and teeth), because they have superior biocompatibility, excellent corrosion resistance, lower Young modulus, higher specific strength and greater working properties in comparison with other metallic implant materials being in use nowadays. In recent years several new β -type titanium alloys made of non-toxic alloying elements such as Nb, Ta and Zr have been developed [1–4], of which the β -type Ti–35Nb–5Ta–7Zr (wt.%) alloy with much lower modulus of elasticity (about 55 GPa) [2] is considered to have great potential to develop into practical applications. Titanium alloys of the β -type have a body centered cubic (bcc) structure and exhibit excellent cold workability [5]. However, their plastic deformation behavior can be very complicated, since various deformation processes, such as slip of dislocations, twinning, stress-induced phase transition or a combination of these processes, might be involved [6]. It has been shown that the deformation behaviors of β -type titanium alloys are closely related to their stability [7–9]. Also, titanium alloys are very susceptible to localized shear deformation which can dominate their deformation behavior under high-strain rate deformation [10]. Localized deformation can have minus effect on the mechani-

cal properties of materials and therefore can lead to catastrophic failure.

So far, many studies referring to the phase transformations, microstructures and mechanical properties have been reported for the Ti–35Nb–5Ta–7Zr alloy [11–13]. However, there are few investigations dealing with the microstructural changes caused by severe plastic deformation. In particular, the information about the structural variations caused by localized deformation in this multi-component alloy is still lacking. The purpose of the present study is to examine the microstructure of the metastable Ti–35Nb–5Ta–7Zr alloy cold-rolled heavily at room temperature, and to characterize structural changes related to deformation localization.

2. Experimental

An alloy ingot with a nominal composition of Ti–35Nb–5Ta–7Zr (wt.%) (referred as “TNIZ” alloy) was prepared by melting high purity metals in the water-cooled copper hearth arc furnace under an argon atmosphere. The obtained ingot was homogenized in vacuum condition at 1273 K for 86.4 ks to eliminate the as-cast microscopic segregation, and was subsequently solution treated at 1273 K for 7.2 ks followed by water quenching. The solution-treated ingot was cut into small pieces, and then some of them were cold rolled to a thickness reduction of 90% via multi-pass process at room temperature without intermediate annealing.

Microstructure observations were carried out using optical microscope (OM). The phase formation was examined with an X-ray diffractometer (XRD) with Cu $K\alpha$ radiation source. Transmission electron microscopy (TEM) and compositional analysis were conducted using a 200 kV field-emission gun electron microscope (JEOL-2010F) equipped with an energy-dispersive X-ray spectroscopy (EDS) system. The samples for TEM observations were prepared by electropolishing with a twin jet electropolisher in a solution of 5 vol% H_2SO_4 , 2 vol% HF and 93 vol% methanol at 35 V and at a temperature of 243 K.

* Corresponding author. Tel.: +86 10 67396167; fax: +86 10 67396167.
E-mail address: weisun@bjut.edu.cn (W. Sun).

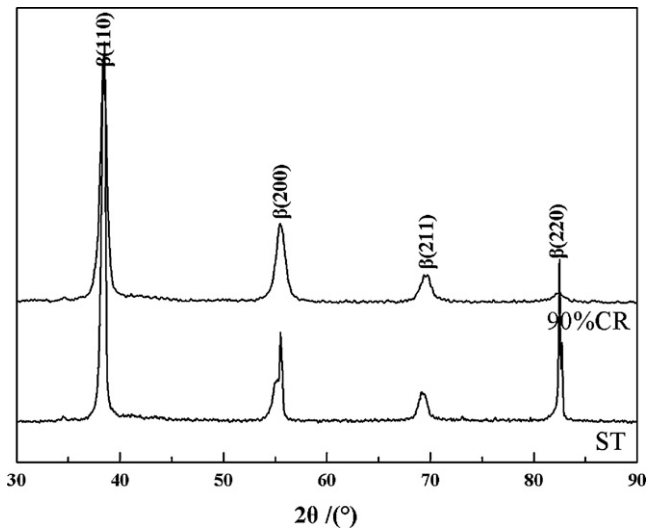


Fig. 1. XRD patterns of the solution-treated (ST) TNTZ alloy and cold-rolled (CR) TNTZ alloy with 90% thickness reduction.

3. Results and discussion

Fig. 1 shows the XRD pattern for the solution-treated TNTZ alloy (ST) and that for the alloy cold-rolled to a 90% reduction (90% CR), respectively. It is clearly shown that both samples have the β phase with a bcc structure as main phase. A small shoulder peak beside the $(200)_{\beta}$ peak in the ST pattern can be indexed as an orthorhombic α'' martensite, indicating the formation of a small amount of α'' martensite during the quenching after the solution treatment. In comparison with diffraction pattern ST for solution-treated TNTZ alloy, diffraction peak broadening exhibiting in the 90% CR pattern can be attributed to grain refinement or residual stress accumulation of high degree during the cold-rolled deformation process. No peaks for secondary phase (such as α'' martensite or ω phase) can be detected after the TNTZ alloy was cold-rolled to 90% reduction.

The microstructural change resulting from the severe cold-rolling deformation is significant. **Fig. 2** shows the optical microstructures for solution-treated and cold-rolled TNTZ alloys.

As can be seen in **Fig. 2(a)**, the solution-treated alloy exhibits a typical equiaxed grain microstructure with only a quite small amount of quenched α'' martensite existing in grain boundary area (indicated with arrow). In contrast, the cold-rolled alloy shows a kind of highly deformed structure which exhibits curved morphology (**Fig. 2(b)**), somewhat similar to the "marble-like" morphology observed in the Gum metal cold-worked by 90% [14]. Since the amount of quenched α'' martensite is so small, its role on the deformation behavior of the solution-treated TNTZ alloy is therefore ignorable.

The details of deformation microstructure in the cold-rolled TNTZ alloy were examined by TEM and by high-resolution transmission electron microscopy (HRTEM) as well. Extensive TEM observations further confirm that the solution-treated TNTZ alloy consists mainly of the bcc β phase and neglectable quenched α'' martensite. **Fig. 3(a)** is a bright-field TEM image taken from the cold-rolled TNTZ alloy with thickness reduction of 90%, showing the formation of dislocation tangle of high density which can result in a complex strain contrast in the β matrix. The viewing direction is along the $[1\ 1\ \bar{3}]_{\beta}$ axis. It is important to point out that, in this region with localized high stress, the formation of stress-induced ω -phases can be detected. The corresponding electron diffraction pattern in **Fig. 3(b)** shows that, in addition to the reflections corresponding to the bcc β matrix phase, extra reflections at the $1/3$ and $2/3$ $\{1\ 1\ 2\}_{\beta}$ positions, which can be indexed as a ω -phase [15], are clearly visible. The high-stress state associating with high-density dislocation tangle is responsible for the pronounced diffuse scattering appearing in the diffraction pattern (see **Fig. 3(b)**). Obviously, the formation of the ω phase coexisting with tangle of high-density dislocation is a result of severe deformation, since no ω phase was found in the solution-treated TNTZ alloy prior to multi-pass cold-rolling deformation. As we have revealed via careful TEM dark-field imaging (see **Fig. 3(c)**), the ω -phases formed in the high-stress region are very fine and have only a few nanometers in size; it is therefore hard to recognize them in the bright-field TEM image exhibiting very complex strain contrast. Also, the formation of the stress-induced ω phase is not detectable in the XRD examination due to its small volume fraction. The detailed study on formation and structure of the stress-induced ω -phase will be reported elsewhere. Here our emphasis will be placed on characterization of the structure of those deformation bands formed by highly localized deformation.

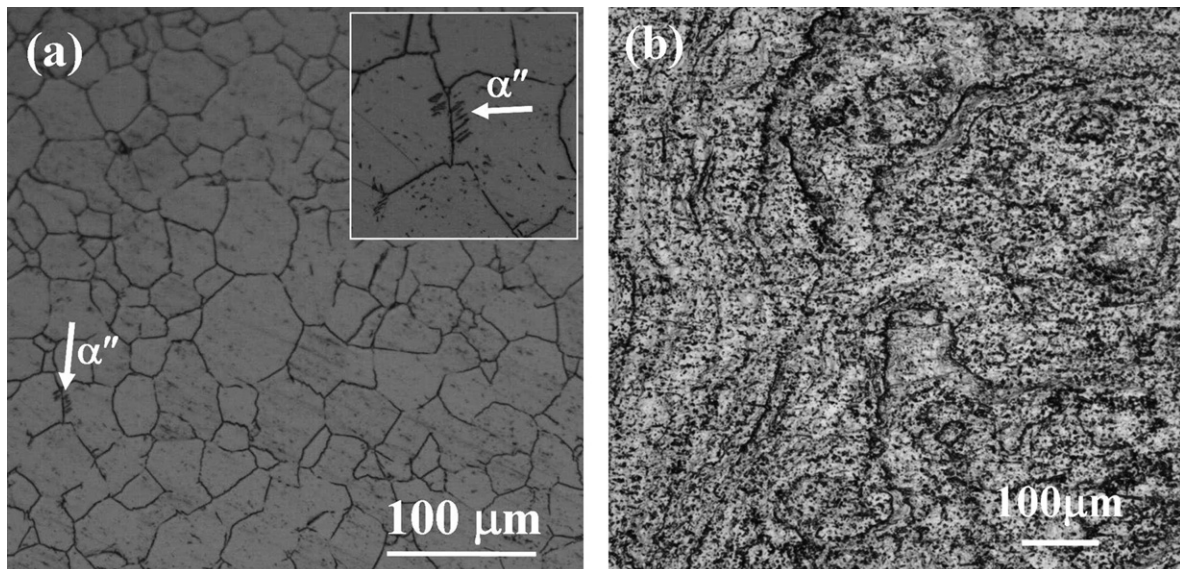


Fig. 2. Optical micrographs of TNTZ alloys: (a) solution-treated and (b) cold rolled to 90% reduction. The inset is an enlarged part of (a), showing the existence of a small amount of quenched α'' martensite near a grain boundary.

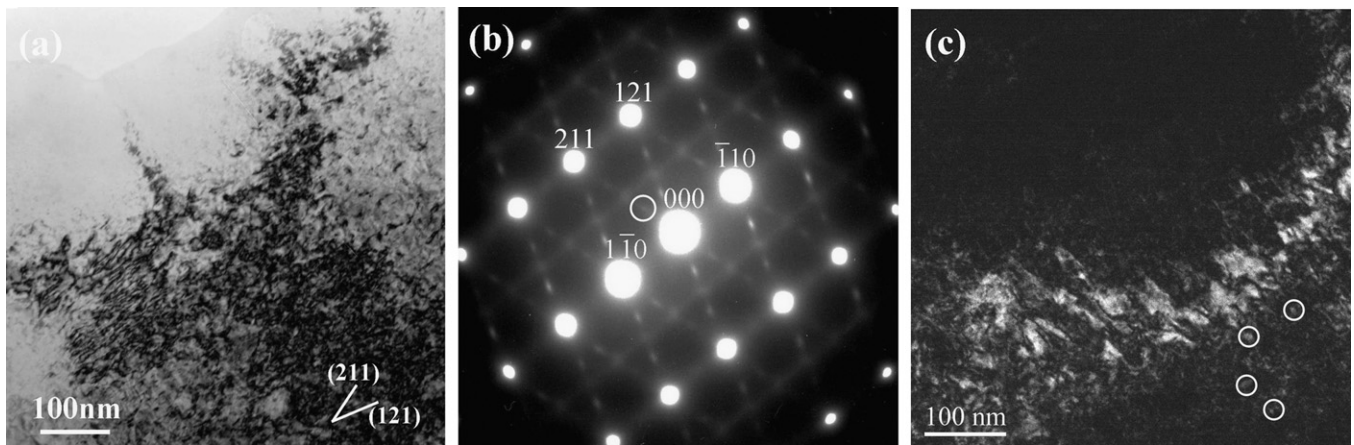


Fig. 3. Bright-field TEM image (a) and the corresponding electron diffraction pattern (b) taken from cold-rolled TNTZ alloy along the $[11\bar{3}]$ axis direction. (c) Dark-field image taken using the $1/3(211)$ reflection, in which nano-sized ω -phases formed in a high stress field are discernible (such as those outlined with white circles).

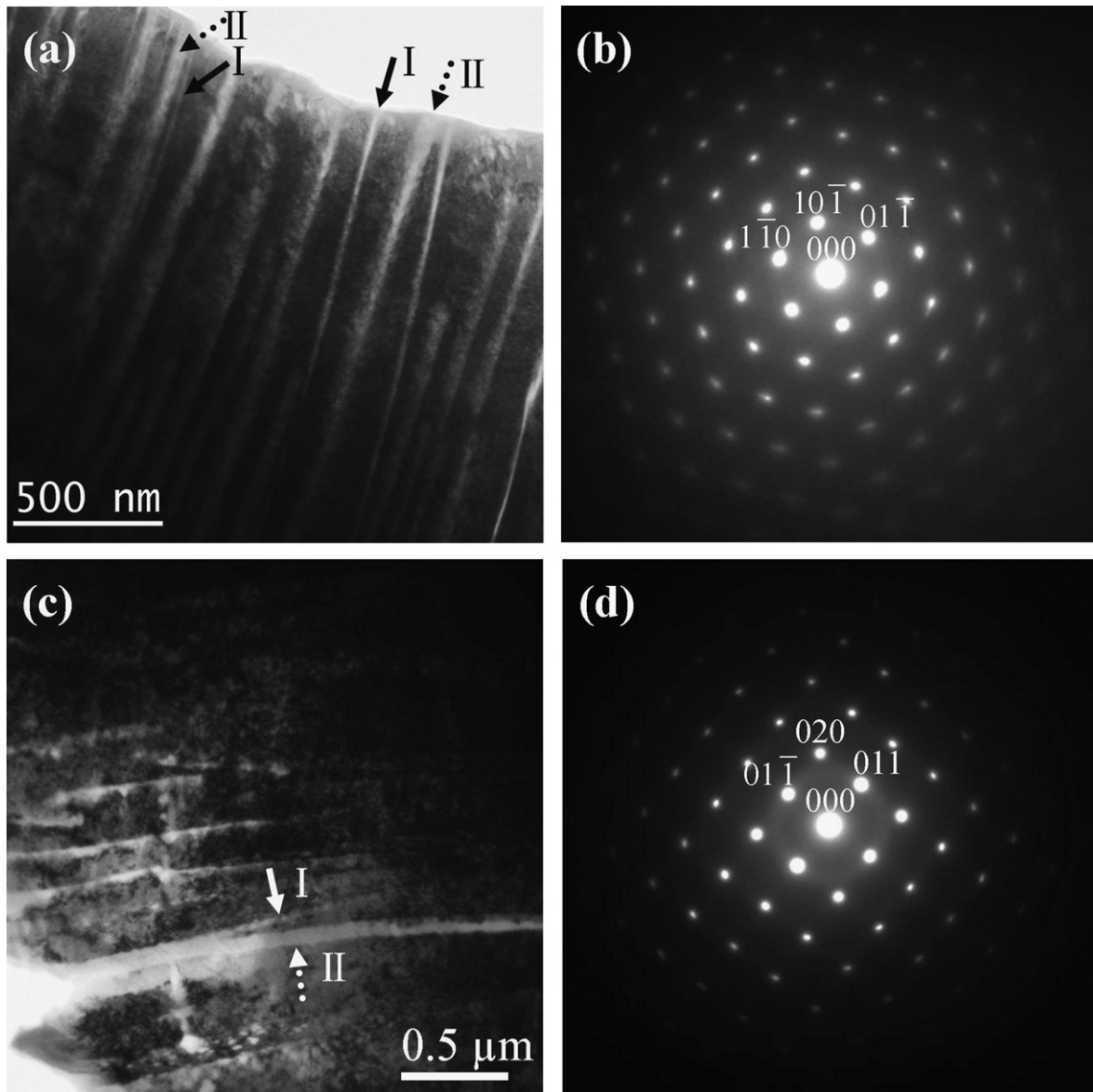


Fig. 4. Bright-field TEM images and their corresponding electron diffraction patterns taken from the cold-rolled TNTZ alloy along (a and b) $[111]_{\beta}$ and (c and d) $[100]_{\beta}$ axis directions, respectively. Note that a halo ring overlapping the $\{110\}$ reflections is clearly discernible in (d), indicating the formation of amorphous structure in deformation bands.

We found that heavy deformation of the TNTZ alloy by cold-rolling resulted in the formation of some long deformation bands along (or close to) basic slip planes. Fig. 4(a) and (c) shows the bright-field TEM images for the TNTZ alloy cold-rolled to 90% reduction, taken along the $[111]_{\beta}$ and $[100]_{\beta}$ axis directions, respectively, in which various deformation bands exhibiting bright contrast are clearly visible. These deformation bands distributed nearly along $\{110\}_{\beta}$ and $\{010\}_{\beta}$ planes when viewed along $[111]_{\beta}$ and $[100]_{\beta}$ directions, and their width and spacing among them are not identical. Two typical morphologies for these deformation bands can be recognized; one represents those narrow, straight bands with strict parallel configuration and clear boundaries, while the other indicates those broad ones with curving configuration and ragged boundaries. Typical deformation bands with these two characteristic morphologies are indicated with solid-line and dashed-line arrows, respectively, in Fig. 4(a) and (c). It should be mentioned that, except for morphology variation of these deformation bands, their bright-contrast features do not undergo obvious change during the sample tilting to different orientations. In this regard, these deformation bands are somewhat like an amorphous structure which can keep a consistent diffraction contrast without depending on the sample orientation. In the electron diffraction patterns presented in Fig. 4(b) and (d) (corresponding to Fig. 4(a) and (c), respectively), the appearance of a weak halo ring passing through $\{110\}$ reflections around the (000) transmission spot can be attributed to the local amorphization occurred within deformation bands. This fact can be proved in the real space as revealed directly by HRTEM observations (see Fig. 5(a)). Neither martensite nor ω -phase can be expected to involve the formation of deformation bands, since no extra reflection can be detected from both matrix and deformation bands in addition to those reflections of the β structure (see Fig. 4(b) and (d)). It should be pointed out that the deformation bands with bright contrast have been observed not only in the thin edge area but also in the thick interior area of the sample. Nano-probe EDS analysis shows that there is no definite compositional difference between the deformation band inside and the nearby β matrix. As can be seen in Fig. 4(a), straight narrow deformation bands are parallel to each other strictly. Note that the bands of this type can form just nearby or even start out directly from broad ones, such as the case indicated with the arrows in Fig. 4(c). It is plausible that those nar-

row and straight deformation bands correspond to “young” ones with a short forming history in comparison with those broad and curving bands with ragged boundaries. It is expectable that these “young” straight bands can merge into the “old” existing bands nearby and contribute to the band widening and amorphization process inside the band through insistent accumulation of high-density defect during the multi-pass rolling. Indeed, those broad and curving deformation bands usually exhibit a more obvious halo ring in the corresponding diffraction patterns (see Fig. 4(c) and (d)).

The structural features inside deformation bands have been directly revealed by HRTEM observations. Localized amorphization has been identified in deformation bands with various morphological features. Fig. 5(a) is the HRTEM image of a straight narrow deformation band taken along the $[111]_{\beta}$ axis direction, showing that its structure is highly defective. FFT pattern from matrix β (A) and that from the deformation band (B) are compared in Fig. 5(c). Actually the highly faulted structure in the deformation band can be described as a kind of mixture consisted of nano-sized β and localized amorphous structures. As indicated with white square “1” in Fig. 5(a), a nano-sized β grain in the deformation band can be clearly seen. This local β structure has a small size (about $4\text{ nm} \times 4\text{ nm}$) and its $[100]_{\beta}$ axis is just parallel to the viewing direction. In addition, other local regions of the β structure with off-zone-axis orientations can also be recognized, such as those indicated with dashed-line circles. Note that no definite boundary can be recognized between the nano-sized β grain and the surrounding amorphous structure. Fig. 5(b) shows the enlarged images from square “1” and “2” in Fig. 5(a), corresponding to local lattice structure inside and outside the deformation band, respectively. Obviously, it is more likely that this distorted local β structure inside the deformation band is a debris part of the original β matrix rather than a recrystallized grain growing from the amorphous surrounding. In this regard, it can be predicted that the thermal generation and its effect on the structural variation during the deformation process can be neglected.

On the other hand, it is important to notice the existence of some in-band residual β which can have significantly large orientation difference with respect to the β matrix outside the deformation band. For instance, the in-band local β structure in square “1” in Fig. 5(b) has a rotation of about 55° with respect to the β matrix (i.e., the angle between $[100]_{\beta}$ and $[111]_{\beta}$ axes). This observa-

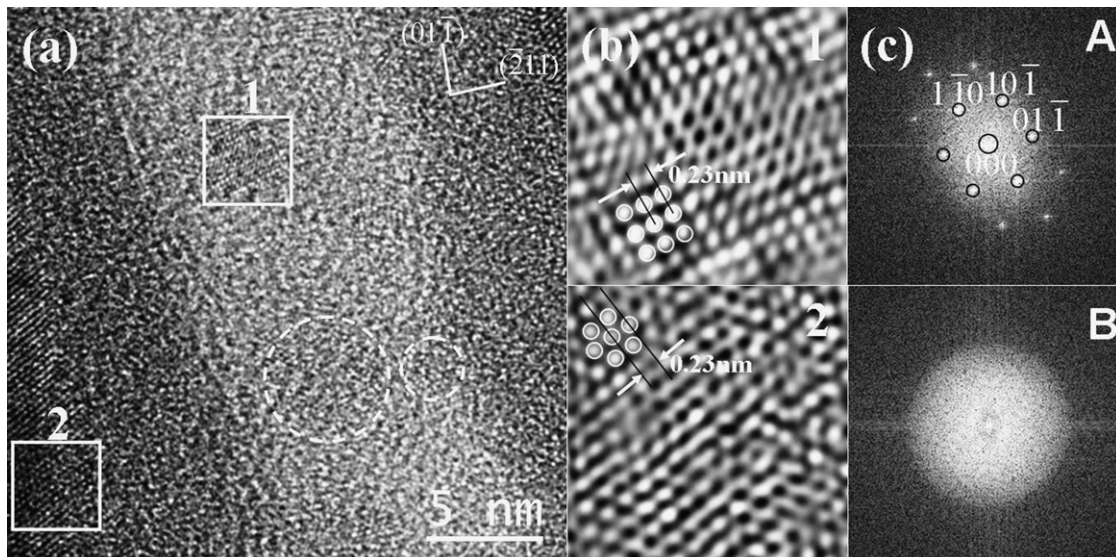


Fig. 5. (a) HRTEM image taken from a typical deformation-band formed in the cold-rolled TNTZ alloy. (b) Enlarged images for areas “1” and “2”, corresponding to a residual β structure in the deformation band and the β matrix, respectively. Both images were filtered through inverse Fourier transform in order to enhance signal-to-noise ratio. (c) FFT patterns corresponding to the β matrix (A) and the deformation band (B).

tion strongly indicates that a deformation band in the TNTZ alloy is actually a localized region subjected to severe deformation during multi-pass rolling. Our results have clearly shown that the structure of the deformation band is highly defective, which is characterized by a mixed structure consisting of part amorphous structure and the residual β structure with small size and different orientations. This is to say, a stress-induced β -to-amorphous transformation must have taken place locally in the deformation band during multi-pass cold-rolling of the TNTZ alloy. It is believed that formation of deformation bands involves the accumulation of high-density dislocations. This process will increase free energy of local region to an extremely high level [16] and finally lead to a bcc β -to-amorphous transformation in high-stress region.

The crystal-to-amorphous transformation caused by cold rolling was first found to occur in the NiTi binary alloy [16], however, the location where the amorphization can occur has not been specified. Recently, Hao et al. have also observed the existence of localized amorphous structure in the compressed Ti–Nb–Zr–Sn alloy [17]. On the whole, however, detailed morphological and structural information involving in the localized amorphization is still lacking. Our results give a clear case showing that crystal-to-amorphous transformation in the TNTZ alloy can take place in deformation bands where the matrix β phase is highly fragmented to a nano size by introducing defects of high density. In fact, this is indeed a very complex process. The detailed study on the crystal-to-amorphous transformation process in deformation bands formed in the TNTZ alloy is still underway and the results will be reported elsewhere.

4. Conclusions

Non-uniform localized deformation microstructures have been observed in the metastable β -type Ti–35Nb–5Ta–7Zr alloy subjected to cold-rolling to 90% reduction. The multi-pass cold rolling of metastable β -type Ti–35Nb–5Ta–7Zr alloy includes various localized deformation processes which can lead to dislocation tangle, stress-induced ω phase transformation and deformation-

band formation. Deformation bands formed during multi-pass cold rolling have different morphological features, whose structures are all characterized by a kind of highly complex mixture consisting of localized amorphous structure and the residual β with nano size and different orientations. The localized amorphization within a deformation band can be attributed to the accumulation of defects of high density caused by severe deformation localization during multi-pass cold-rolling.

Acknowledgement

This work is financially supported by Science and Technology General Program Foundation of Education Committee of Beijing under Grant No. KM200810005029.

References

- [1] M. Niinomi, Mater. Sci. Eng. A 243 (1998) 231–236.
- [2] M. Long, H.J. Rack, Biomaterials 19 (1998) 1621–1639.
- [3] G.J. Yang, T. Zhang, J. Alloys Compd. 32 (2005) 291–294.
- [4] L.Q. Wang, W.J. Lu, J.N. Qin, F. Zhang, D. Zhang, J. Alloys Compd. 469 (2009) 512–518.
- [5] L.Q. Wang, W.J. Lu, J.N. Qin, F. Zhang, D. Zhang, Mater. Trans. 49 (2008) 1791–1795.
- [6] T.S. Kuan, R.R. Ahrens, S.L. Sass, Metall. Trans. A 6 (1975) 1767–1774.
- [7] W. Xu, K.B. Kim, J. Das, M. Calin, J. Eckert, Scripta Mater. 54 (2006) 1943–1948.
- [8] H. Xing, J. Sun, Appl. Phys. Lett. 93 (2008) 031908.
- [9] Y. Yang, G.P. Li, G.M. Cheng, Y.L. Li, K. Yang, Appl. Phys. Lett. 94 (2009) 061901.
- [10] Y.B. Xu, Y.L. Bai, M.A. Meyers, J. Mater. Sci. Technol. 22 (2006) 737–746.
- [11] X. Tang, T. Ahmed, H.J. Rack, J. Mater. Sci. 35 (2000) 1805–1811.
- [12] L.M. Elias, S.G. Schneider, S. Schneider, H.M. Silva, F. Malvisi, Mater. Sci. Eng. A 432 (2006) 108–112.
- [13] P.L. Ferrandini, F.F. Cardoso, S.A. Souza, C.R. Afonso, R. Caram, J. Alloys Compd. 433 (2007) 207–210.
- [14] T. Saito, T. Furuta, J.H. Hwang, S. Kuramoto, K. Nishino, N. Suzuki, R. Chen, A. Yamada, K. Ito, Y. Seno, T. Nonaka, H. Ikehata, N. Nagasako, C. Iwamoto, Y. Ikuhara, T. Sakuma, Science 300 (2003) 464–467.
- [15] R. Banerjee, P.C. Collins, D. Bhattacharyya, S. Banerjee, H.L. Fraser, Acta Mater. 51 (2003) 3277–3292.
- [16] J. Koike, D.M. Parkin, M. Nastasi, J. Mater. Res. 5 (1990) 1414–1418.
- [17] Y.L. Hao, S.J. Li, B.B. Sun, M.L. Sui, R. Yang, Phys. Rev. Lett. 98 (2007) 216405.